

A PROCESS-STRUCTURE-PROPERTY-PERFORMANCE FRAMEWORK FOR DIGITAL ENGINEERING-ENABLED REPAIR OF ALUMINUM PARTS

Jim Lua[1], Manoj R. Rajanna[1], Hang Yu[2], Alan Timmons[3], Gabriel Murray[3], & Nam Phan[3]

[1]Global Engineering & Materials, Inc., Princeton, New Jersey, USA
[2]Virginia Tech, Blacksburg, Virginia, USA
[3]Naval Air Systems Command (NAVAIR), Patuxent River, Maryland, USA

Abstract

A multiphysics process–structure–property–performance (PSPP) framework was developed for additive friction stir deposition (AFSD) repair of AA7050 aluminum alloy. The framework integrates sequentially coupled models for thermal-fluid dynamics, microstructure evolution, heterogeneous mechanical properties, and fatigue performance, enabling prediction of the complex thermal, metallurgical, and mechanical phenomena governing the AFSD process. The PSPP framework was validated using AFSD hole-repair experiments conducted at a tool rotational speed of 350 RPM. Good agreement was achieved between model predictions and experimental measurements of temperature history, material flow, microstructural evolution, formation of distinct material zones, and fatigue crack initiation behavior. The validated framework was subsequently applied to investigate the effect of tool rotational speed on precipitate evolution and fatigue performance. Simulations were performed at rotational speeds of 235, 250, and 350 RPM. The results showed that increasing rotational speed increased thermal exposure, resulting in enhanced precipitate dissolution and coarsening, reduced resistance to dislocation motion, and higher fatigue indicator parameter (FIP) values. Consequently, the predicted fatigue crack initiation life decreased from approximately 19,800 cycles at 235 RPM to 10,800 cycles at 350 RPM. The superior fatigue performance at 235 RPM was attributed to the retention of fine strengthening precipitates and the associated increase in slip resistance. These results demonstrate the critical role of process-induced precipitate evolution in controlling the fatigue performance of AFSD-repaired AA7050 structures. The proposed PSPP framework provides a physics-based tool for process optimization and tailoring, enabling rapid selection of processing conditions that maximize fatigue performance while minimizing process-induced defects.

Keywords: keywords Aluminum alloy, hole repair, additive friction stir deposition, process-structure-property-performance (PSPP), fatigue life

1. Introduction

High-strength 7xxx-series aluminum alloys, such as AA7050, are widely used in aerospace structures because of their high specific strength, fracture toughness, and fatigue resistance. Components fabricated from these alloys are frequently exposed to cyclic loading, corrosive environments, and accidental damage during service, which can lead to crack initiation, material loss, and structural degradation. Corrosion maintenance and control are major contributors to sustainment costs and reduced fleet availability. In particular, damage to fastener holes in AA7050 structures presents a significant challenge to aircraft longevity, and conventional bushing methods for repairing oversized holes are often inadequate because they do not provide metallurgical bonding. Replacing damaged components can be difficult or impractical due to system complexity, limited material availability, and legacy design constraints. Even when replacement parts are available, the downtime associated with component removal, replacement, and recertification can adversely affect aircraft availability and mission readiness [1].

Repairs can generally be classified as either cosmetic or structural. Cosmetic repairs focus

primarily on restoring the original geometry, whereas structural repairs must restore both the geometry and the mechanical performance of the component. The quality and effectiveness of a structural repair depend on several factors, including the properties of the deposited material, the metallurgical integrity and strength of the interface between the repair material and the substrate, the extent of microstructural and mechanical property changes in the surrounding base material, and the dimensional accuracy of the repaired region relative to the original component geometry [2,3].

Structural repair methods based on either fusion-based or solid-state processing aim to restore the original geometry while achieving the required post-repair mechanical performance. Unlike conventional fusion-based additive manufacturing (AM) processes [4,5], additive friction stir deposition (AFSD) does not involve melting and solidification of the material. Consequently, defects commonly associated with fusion-based processes, such as lack of fusion, solidification cracking, porosity, keyholing, and high residual stresses, can be significantly reduced or eliminated. AFSD combines the friction stir principle with a material-feeding mechanism to enable location-specific material deposition for structural repair, producing strong metallurgical bonding and fine equiaxed microstructures within the stir zone [6–8]. Additional benefits of AFSD arise from the severe plastic deformation and elevated temperatures experienced during deposition, which promote dynamic recrystallization and typically result in refined microstructures with wrought-like mechanical properties [9]. Furthermore, strong metallurgical bonding can be established between the deposited material and the substrate, eliminating the weak interfaces often associated with conventional repair methods. Recent studies have demonstrated the capability of AFSD to produce deposited aerospace aluminum alloys with wrought-like properties [10] and to successfully repair defects such as linear grooves [11] and through-holes [12].

The mechanical performance of AFSD-repaired components is strongly influenced by the distribution of process-induced defects and the microstructure-dependent constitutive behavior of the repaired material. Because AA7050 is a precipitation-hardened aluminum alloy, the rapid thermal cycles experienced during AFSD can lead to the dissolution, reprecipitation, and coarsening of strengthening precipitates. The evolution of the microstructure through the precipitation sequence, supersaturated solid solution (SSS) → GP zones → η′ → η, plays a critical role in determining the yield strength, ductility, and fatigue performance of the repaired material [13,14].

From a fatigue-performance perspective, the most influential microstructural feature is not grain refinement alone, but rather the evolution of the strengthening η′ precipitates and grain-boundary η precipitates. Excessive heat input during AFSD can promote the dissolution of η′ precipitates and the coarsening of grain-boundary η precipitates, reducing resistance to dislocation motion and increasing cyclic plastic deformation. Consequently, fatigue damage accumulates more rapidly, resulting in reduced crack initiation life. Thus, higher heat input may produce a finer recrystallized grain structure while simultaneously degrading fatigue performance due to unfavorable precipitate evolution.

Although AFSD offers significant flexibility for tailoring microstructure through the control of process parameters, feedstock characteristics, and external thermal conditions during and after deposition, identifying an optimal repair strategy through experimental trial-and-error remains costly and time-consuming due to the high-dimensional process–microstructure–property-performance design space. For a given damage configuration and performance requirement, it is therefore essential to rapidly identify an operational process window and associated thermal boundary conditions that minimize process-induced defects while achieving the desired mechanical performance. Accomplishing this objective requires a validated virtual testing framework capable of capturing the coupled thermal, mechanical, metallurgical, and microstructural phenomena that govern the evolution of microstructure, material properties, and structural performance during AFSD repair.

To establish process–structure–property relationships for AFSD-repaired aluminum components, several advanced modeling strategies have been developed. These include smooth particle hydrodynamics (SPH), which can capture the large deformations, material flow, and local thermomechanical histories that govern microstructural evolution and mechanical performance [8,15]. Because AFSD shares many similarities with friction stir welding (FSW), computational solid

mechanics approaches that do not explicitly account for material flow have also been incorporated into process–structure–property integrated computational materials engineering (ICME) frameworks to predict the mechanical properties of AFSD-repaired AA7050 components [16].

However, the large material flow inherent to AFSD plays a critical role in determining stir-zone geometry, material mixing, interfacial bonding quality, and defect formation. Consequently, high-fidelity AFSD process simulations must explicitly account for severe plastic deformation and material transport to accurately capture the thermal and mechanical histories that govern microstructural evolution and repair performance.

While SPH is well suited for modeling large material deformation without mesh distortion, its application to realistic AFSD repair scenarios remains computationally expensive because of the large number of particles required, small stable time increments, and the use of explicit time integration. Alternatively, computational fluid dynamics (CFD) approaches can efficiently simulate material flow, large deformation, temperature evolution, and strain-rate distributions at a significantly lower computational cost [17]. Although the contact pressure predicted by CFD-based AFSD models is generally less accurate than that obtained from SPH simulations, the associated frictional heat generation can be improved through calibration of the contact pressure and frictional traction. Furthermore, as an inherently Eulerian formulation, CFD eliminates mesh distortion and convergence issues associated with severe deformation, making it particularly attractive for process optimization and parametric studies involving multiple design variables.

Despite substantial progress in modeling friction-stir-based processes, including process simulation, microstructural evolution, and property prediction, the capability to establish a comprehensive process–structure–property–performance (PSPP) framework for the optimization and tailoring of AFSD-based repair and fabrication of AA7050 components remains limited. This limitation stems primarily from the strongly coupled multiphysics and multiscale nature of the AFSD process, which links thermal history, material flow, dynamic recrystallization, precipitation evolution, heterogeneous mechanical properties, and ultimately fatigue performance. As a result, accurate prediction of repair quality and structural performance requires an integrated modeling framework capable of capturing the complex interactions among process conditions, microstructure evolution, material properties, and fatigue behavior.

In this work, a multiphysics modeling framework is developed to establish the process–structure–property–performance (PSPP) linkage for AFSD-repaired aluminum components. The physics-based framework captures the key coupled phenomena governing repair performance, including material flow, plastic deformation, dynamic recrystallization, thermal history, precipitation dissolution and coarsening, formation of distinct material zones, and fatigue crack initiation and propagation.

The integrated PSPP framework sequentially couples a CFD-based process model for predicting temperature, material flow, and strain-rate fields; microstructure evolution models for characterizing dynamic recrystallization, grain structure evolution, and precipitate kinetics; a representative volume element (RVE)-based crystal plasticity model for determining local mechanical properties and fatigue indicator parameters (FIPs); and a fatigue performance model for predicting crack initiation and crack growth life. Together, these solution modules establish a quantitative linkage between AFSD process parameters, microstructural evolution, and structural performance.

The predictive capability of the PSPP framework is first validated through comparisons between model predictions and experimental measurements obtained from AFSD-repaired AA7050 hole coupons fabricated at a tool rotational speed of 350 RPM. The validated framework is subsequently applied to investigate the influence of tool rotational speed on precipitate evolution and fatigue performance and to identify process conditions that maximize fatigue crack initiation life. The results demonstrate the capability of the PSPP approach to enable physics-informed optimization of AFSD repair parameters and provide a foundation for future digital engineering-enabled design, qualification, and manufacturing of high-performance aluminum components.

2. Process-Structure-Property-Performance (PSPP) Methodology

2.1 Overview

In this study, we developed an integrated process–structure–property–performance (PSPP) modeling framework shown in Figure 1 for additive friction stir deposition (AFSD) repair of aluminum alloy 7050. As shown in Figure 1, the PSPP toolkit for AFSD repair and fabrication analysis consists

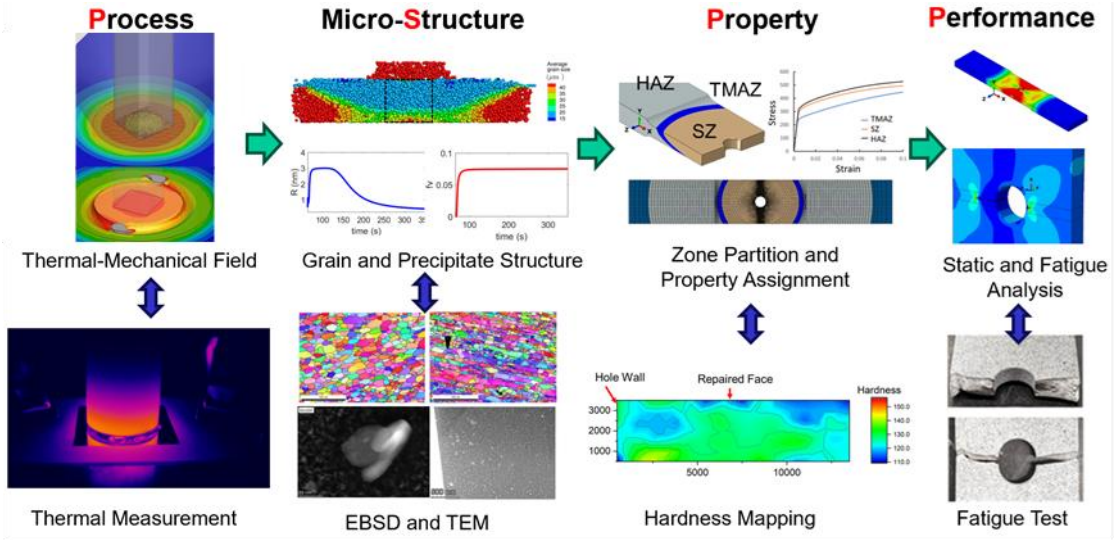


Figure 1 – PSPP modeling framework for establishing the process-structure-property-performance relationships in AFSD hole repair.

of: (1) a high-fidelity computational fluid dynamics (CFD)-based process model that captures thermal response, plastic flow, material mixing, and tool–workpiece interactions; (2) a microstructure evolution and multi-stage precipitation model that predicts grain size and precipitate distributions based on the thermal history and material flow behavior; (3) a digital constitutive model based on crystal plasticity that generates local stress–strain relationships for the dynamically recrystallized zone (DRXZ), thermo-mechanically affected zone (TMAZ), heat-affected zone (HAZ), and base material (BM) from the heterogeneous microstructure; (4) a customized Abaqus-based performance evaluation model incorporating zone mapping, bond interfaces, and initial flaws at stress concentration sites for crack propagation prediction; and (5) a total-life prediction model that captures microstructure-driven crack initiation using fatigue indicator parameters (FIPs).

2.2 CFD-based Process Modeling for Thermal and Material Flow Prediction

We implemented a CFD-based process model for AFSD through customization of the Star-CCM+ software. In this approach, the material is treated as a non-Newtonian viscoplastic fluid, while elastic and strain-hardening effects are neglected. The temperature and velocity fields are solved using computational fluid dynamics (CFD) methods. The normal pressure and frictional forces at the tool–workpiece interface are calibrated to accurately predict heat generation during the process. A key advantage of the CFD approach is its Eulerian formulation, which eliminates mesh distortion and convergence issues associated with severe material deformation. As a result, CFD models are computationally efficient and robust for simulating AFSD processes. The Volume of Fluid (VOF) method is employed to track material feeding, deposition, and spreading.

As shown in Figure 2, the Navier–Stokes (*NS*) equations governing the conservation of mass, momentum, and energy are solved, where v is the velocity, ρ is the density, p is the pressure, τ is the viscous stress tensor, c_p is the specific heat, T is the temperature, k is the thermal conductivity, $\dot{S}_{vis}$ is the heat generation due to plastic deformation, and t is time. The viscoplastic constitutive behavior is incorporated into the viscous stress tensor, τ, as illustrated in Figure 2. The flow stress (σ_f) is modeled as a function of temperature and strain rate, while strain-hardening effects are neglected. This assumption is based on the large plastic strains experienced during AFSD, under which the influence of accumulated strain on the flow stress is considered secondary compared with the effects of temperature and strain rate.

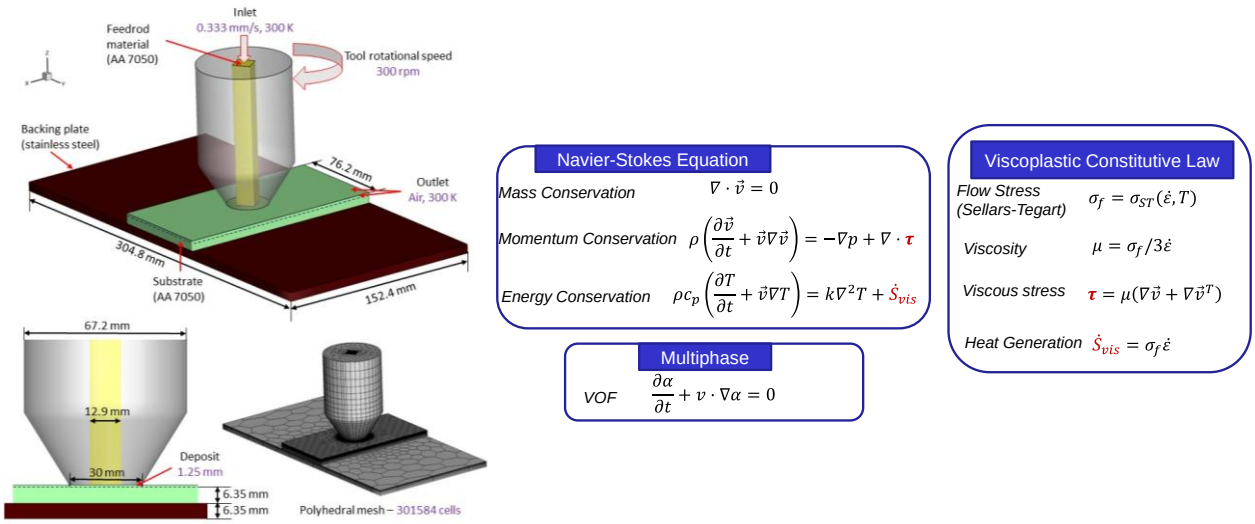


Figure 2 – Summary of key components used in CFD-based process model for multidomain AFSD simulation.

A significant amount of effort was devoted to defining the boundary conditions at the interface between the steel tool and the aluminum alloy workpiece. It is assumed that the workpiece material can exist in either a sticking or sliding state. In the sticking state, the workpiece moves at the same velocity as the tool ($v_{wp}=v_{tool}$). In the sliding state, the workpiece moves at a lower velocity than the tool ($v_{wp}<v_{tool}$). To achieve more accurate predictions during the transient stage of the repair process, the Volume of Fluid (*VOF*) method was employed to track material feeding and the evolution of the material–air interface. The *VOF* method uses a scalar volume fraction function, α, to distinguish between the viscoplastic metal and air phases. The *VOF* function is governed by the advection equation shown in Figure 2, where $\alpha = 0$ represents the air phase and $\alpha = 1$ represents the metal phase. It should be noted that the air phase is treated as a dummy phase in the *CFD* calculations. Its sole purpose is to track the flow of feedstock material into the repair region and its spreading across the tool surface. The governing equations and constitutive relationships described previously are applied only in regions where $\alpha = 1$, while air properties are assigned to regions where $\alpha = 0$.

As illustrated in Figure 1, material is extruded from the feed rod, spread across the tool surface, and deposited onto the substrate. Initially, contact between the tool shoulder and the workpiece is characterized by a sliding condition. As the temperature increases and the material softens, a sticking condition is gradually established, causing the deposited material to rotate with the tool and enhancing material transport and mixing within the deposition zone.

2.3 Process-Structure Linking and Microstructure Modeling

The integration of process modeling with microstructure modeling through Lagrangian particle tracking (*LPT*) is an essential approach to understanding the evolution of materials during the AFSD processes. *CFD* simulations provide Eulerian field data, such as velocity, temperature, and strain rate. However, the microstructure evolution is associated with each material point described by the Lagrangian method. As shown in Figure 1, The *LPT* method allows us to simulate the trajectories of discrete particles as they move through the fluid, responding to the AFSD processing conditions. By leveraging the velocity information obtained from *CFD* simulations, we can calculate the new positions of these particles over time, effectively mapping their motions through the processing environment. Furthermore, using the strain rate data, we can deduce how particles deform and experience strain as they interact with the fluid flow. The implemented numerical solution procedure includes 1) initialization of the individual particles' locations in the area of interests at time of $t=0$; 2) interpolation and mapping the data such as velocity, strain rate, and temperature obtained from the *CFD* simulation at $t=t+\Delta t$; 3) calculation of the new positions of the particles using $X_{new} = X_{old} + V\,dt$; 4) determination of the corresponding strain for each particle using $\varepsilon = \varepsilon + \dot{\varepsilon}\,dt$; and 5) repetition of Step 2 to 4 to track the particles for the entire AFSD

process over time.

2.4 Microstructure Evolution and Property Prediction

The outputs from the process model are the temperature and strain-rate fields as functions of time, ($T(x,y,z,t)$) and $\dot{\varepsilon}(x,y,z,t)$). These thermo-mechanical fields are used to predict grain and precipitate evolution during the AFSD process. The primary mechanism governing grain evolution is dynamic recrystallization (DRX). A physics-based modeling framework was developed to describe the grain refinement process. Continuous dynamic recrystallization (*CDRX*) refers to the process in which dislocations actively migrate during severe plastic deformation at elevated temperatures. The accumulation and rearrangement of dislocations promote the formation of subgrains, which gradually evolve into new fine grains that replace the original coarse grains. Geometric dynamic recrystallization (*GDRX*) occurs when grain deformation becomes sufficiently severe that elongated grains are pinched off, resulting in the formation of smaller recrystallized grains. To capture this mechanism, the model computes the distance between grain boundaries, (D_{GB}), and the subgrain size, (D_{SG}). When (D_{GB}) becomes smaller than (D_{SG}), the subgrains separate from the elongated grains, indicating the onset of *GDRX*. This process leads to significant grain refinement within the dynamically recrystallized zone. By combining the effects of *CDRX* and *GDRX*, the model predicts the evolution of grain size and morphology as functions of the local thermal and deformation histories experienced during the AFSD process.

A precipitate evolution model based on the Kampmann–Wagner Numerical (KWN) framework was developed using a thermodynamic description of homogeneous precipitation, as described in [18]. The model takes as input the alloy chemical composition, the diffusion coefficients of the solute elements in the matrix, and the thermodynamic and compositional information of the precipitate phases. Using these inputs, the model predicts the nucleation, growth, coarsening, and dissolution of precipitates during the thermal cycles experienced in the AFSD process. The primary outputs of the model are the precipitate size distribution, average precipitate radius, and precipitate volume fraction as functions of time and temperature. These predictions provide critical information for evaluating the evolution of microstructure and its influence on the local mechanical properties of the deposited material.

After determining the microstructure across the AFSD-repaired regions based on the CFD-predicted temperature and strain-rate fields, a physics-based crystal plasticity constitutive model was developed to incorporate the effects of key microstructural features, including grain size, precipitate size and volume fraction, and dislocation density, following the framework described in [19]. Digital constitutive properties are generated for each distinct microstructural zone formed during the AFSD process. These zones include: (1) the dynamically recrystallized zone (DRXZ), where severe plastic deformation induced by the AFSD tool results in the formation of fine, equiaxed recrystallized grains; (2) the thermo-mechanically affected zone (TMAZ), where significant plastic deformation produces a high dislocation density and alters the microstructure without complete recrystallization; (3) the heat-affected zone (HAZ), where little or no plastic deformation occurs, but thermal exposure leads to precipitate coarsening and overaging; and (4) the base material (BM), which retains its original microstructure and mechanical properties. The crystal plasticity model utilizes the predicted microstructural attributes within each zone to establish local stress–strain relationships, thereby providing a direct linkage between process-induced microstructural evolution and the resulting mechanical behavior of the repaired structure.

2.5 Performance Modeling Based on Damage Initiation and Crack Propagation

A multi-stage fatigue life (MSF) model was developed based on the framework proposed by McDowell [20] to incorporate the effects of microstructural features on the fatigue behavior of AFSD-repaired Al7050. The fatigue life can be divided into three distinct stages: fatigue crack initiation (incubation), small-crack growth, and long-crack growth. The MSF model treats each stage as a separate damage regime and sums their individual contributions to determine the total fatigue life. The fatigue crack initiation life is predicted using fatigue indicator parameters (FIPs) obtained from crystal plasticity finite element simulations of a representative volume element (RVE). The FIPs are based on microstructure-sensitive quantities such as accumulated plastic slip

and/or accumulated energy dissipation, which are directly related to the local deformation mechanisms responsible for fatigue damage initiation. The small-crack growth stage is modeled using a crack-tip-opening-displacement (CTOD)-based approach to capture the influence of microstructural barriers and local plasticity on crack propagation. Once the crack reaches a sufficient size for continuum fracture mechanics assumptions to become valid, the long-crack growth stage is modeled using Paris' law within the framework of linear elastic fracture mechanics (LEFM). To predict the fatigue crack growth life and crack propagation path in AFSD-repaired structures, we utilized XFA3D, an add-on toolkit for ABAQUS [21, 22], which is based on the three-dimensional extended finite element method (3D XFEM). The XFEM approach enables crack initiation and propagation to be modeled independently of the finite element mesh, thereby allowing efficient simulation of complex crack-growth behavior without the need for repeated remeshing.

3. PSPP Tool Validation for AFSD Hole Repair Simulation at 350 RPM

3.1 Problem Description

As shown in Figure 3, the feed rod and print head rotate simultaneously at high speed to enable rapid heating and severe plastic deformation of the metallic feedstock. Frictional heating occurs when the feed material comes into contact with the substrate, causing the material to soften and flow under the combined compressive and shear forces imposed by the feeding system and rotating print head.

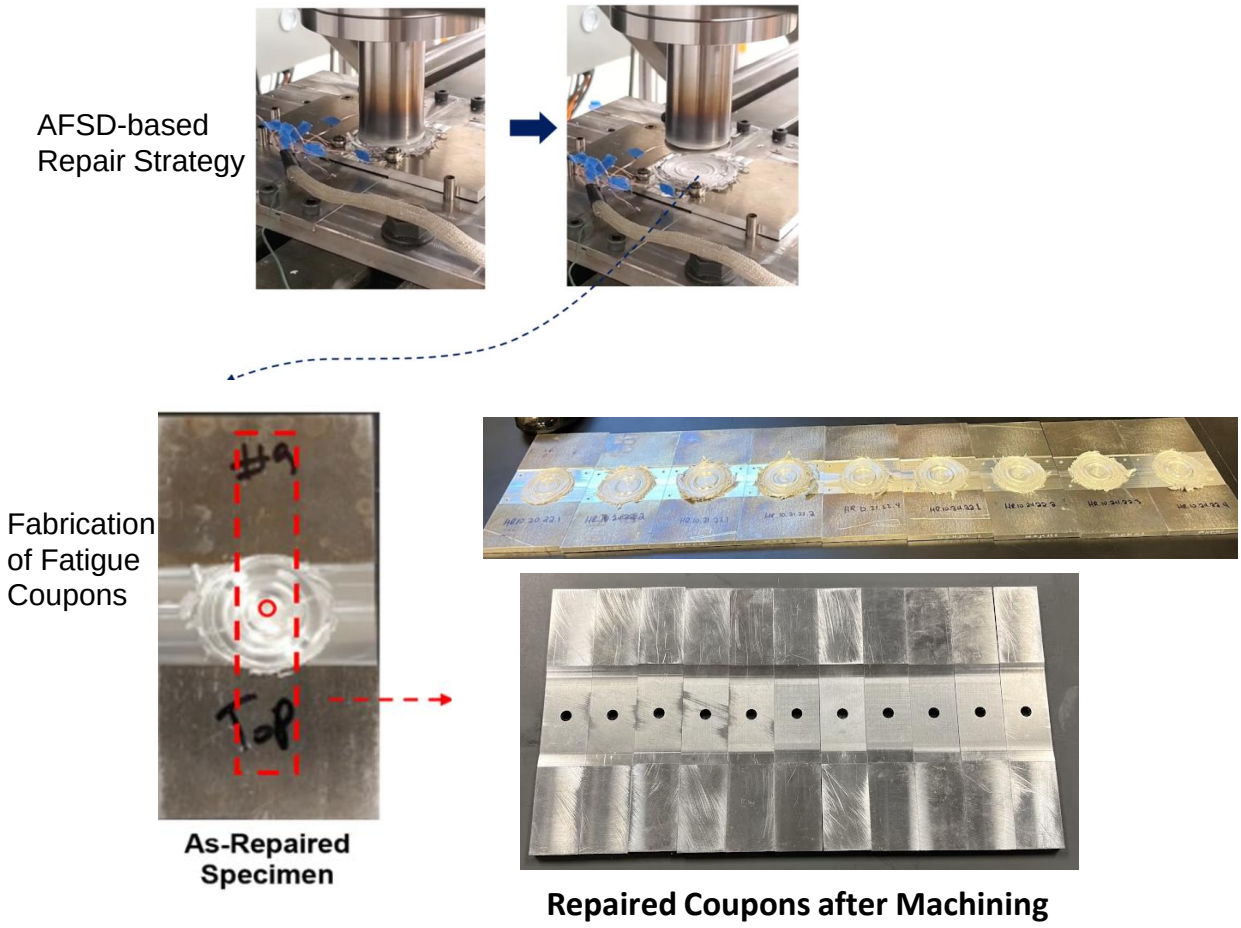


Figure 3 – Experimental setup for AFSD-based hole repair and fabrication of repaired coupons for performance evaluation.

During the deposition process, not only does the feed material undergo significant plastic deformation, but the surface layers of the substrate also plastically deform and mix with the deposited material, resulting in a strong metallurgical bond. With this deformation-assisted interfacial bonding, the in-plane motion of the print head can be controlled through the G-code to deposit material in an arbitrary pattern within a given layer. The tool path and feed rate are carefully

controlled to ensure complete filling of the oversized hole with AA7050 material. Figure 3 illustrates the AFSD process used to fully repair an oversized hole with a diameter of 7.94 mm in a 6.35-mm-thick AA7050 plate, along with an image of the top surface of an as-filled coupon. Following deposition, the excess material was removed by machining, and a hole with the original diameter of 6.35 mm was subsequently drilled at the center of the repaired region. Fatigue tests were conducted on the repaired coupons under fully reversed loading conditions with a load ratio, R, of −1, as shown in Figure 4.

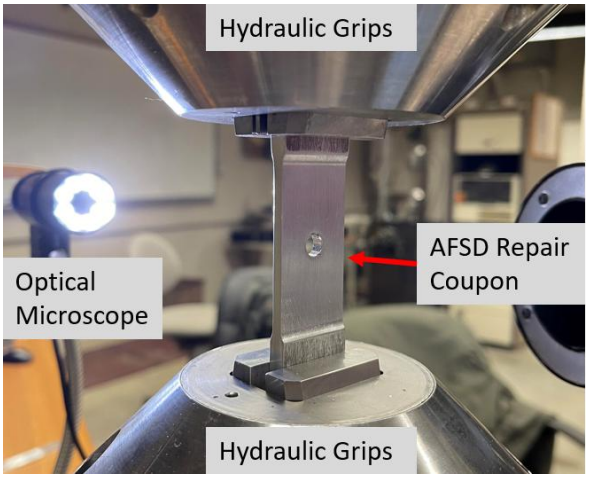


Figure 4 – Fatigue setup for performance evaluation of AFSD hole-repaired coupons.

The repair quality and fatigue performance are strongly governed by the AFSD processing conditions, including print head rotational speed, material feed rate, dwell time, and print path. To investigate the dominant effects of tool rotational speed, hole-repair coupons were fabricated using low, high, and optimized RPM setpoints, followed by fatigue testing to examine the influence of print head rotational speed on the failure mechanisms and cycles to failure (CTF). A schematic illustration is provided to demonstrate the repair-quality-dependent failure mechanisms. At low RPM, insufficient penetration, material mixing, and metallurgical bonding through the thickness of the hole can result in incomplete filling of the repair region, leading to reduced fatigue life. At high RPM values beyond the optimum condition, excessive heat input can dissolve fine strengthening precipitates and promote the formation of coarser precipitates during cooling. This microstructural degradation reduces the yield strength, lowers the resistance to cyclic deformation, and accelerates fatigue crack initiation.

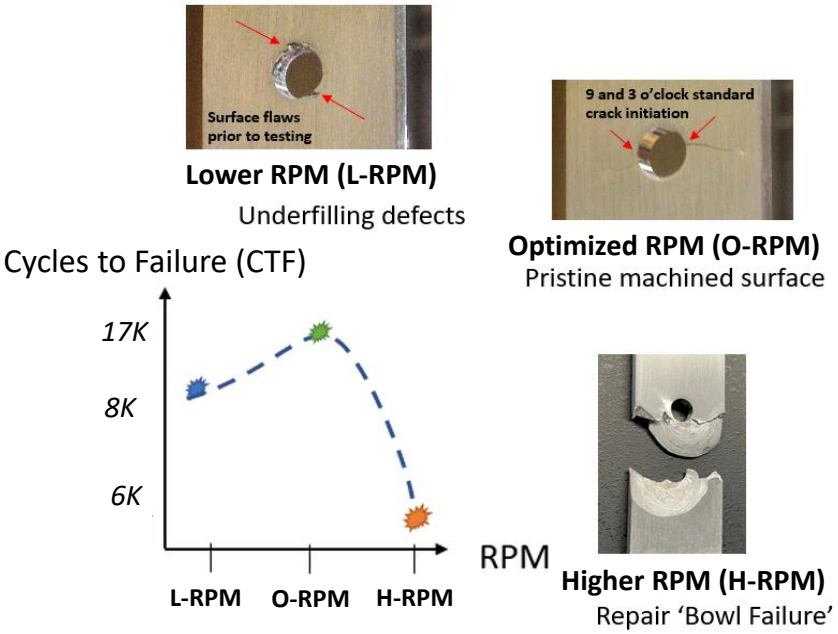


Figure 5 – Schematic illustration of the effects of tool rotational speed on failure mode, repair feature filling, and fatigue life.

As shown in Figure 5, a normal failure mode is observed for specimens repaired at the optimized RPM, where fatigue cracks initiate and propagate from approximately the 3 o'clock and 9 o'clock positions of the hole. In contrast, an irregular failure mode is observed at high RPM, driven by delamination along the thermally degraded metallurgical interface within the repaired region. This observation further motivates the use of the PSPP framework for process tailoring and optimization to improve the fatigue performance of AFSD-repaired hole coupons.

Given the strong temperature dependence of microstructural evolution and the resulting property gradients between the stir zone and the base material, thermocouples were installed in hole-repair coupons fabricated at a high tool rotational speed to collect in-situ temperature data for validation of the thermal-CFD process model. In addition, optical microscopy and EBSD characterization were performed to identify the distinct material zones and their associated microstructures, which were subsequently used to validate the microstructural evolution model predictions. For AFSD-repaired AA7050 hole coupons, a significant portion of the fatigue life is spent in the microstructurally short-crack and physically short-crack growth regimes. Therefore, it is essential to employ a microstructure-based fatigue indicator parameter (FIP) to predict the crack initiation life, which is estimated to account for approximately 80% of the total fatigue life. Accurate prediction of crack initiation is particularly important because local microstructural features, residual stresses, and cyclic plastic deformation strongly influence the nucleation and early growth of fatigue cracks within the repaired region.

All AFSD hole-repair experiments were conducted at Virginia Tech using their L3 MELD AFSD system. In the following sections, validation studies are presented for each solution module at a tool rotational speed of 350 RPM, including temperature prediction, microstructural evolution, material property characterization, and fatigue performance. The validated PSPP framework is then used to demonstrate process tailoring and optimization for improved repair performance.

3.2 Verification of CFD-Based Process Simulation Model

We first compare the temperature predictions from the process simulations with thermocouple measurements obtained during the hole-repair process. An illustration of the experimental setup, along with the locations of the thermocouples (TCs), is shown in Fig. 6. The test coupon consisted of an AA7050 substrate measuring 76.2 mm × 152.4 mm × 6.35 mm with a centrally located hole of 7.94 mm diameter. The coupon was positioned on top of a large steel backing plate.

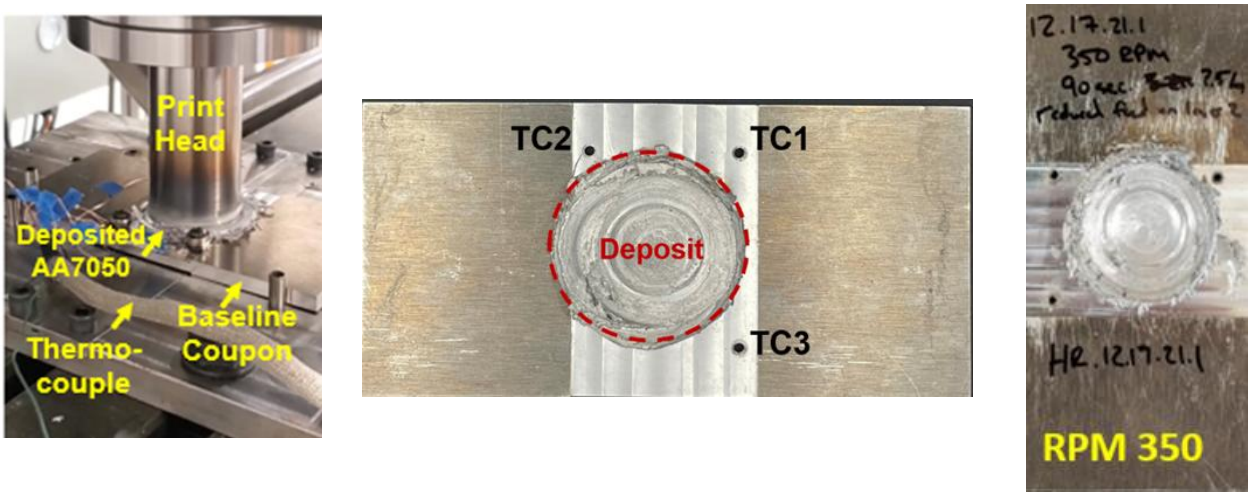


Figure 6 – AFSD hole-repair setup and thermocouple locations for AA7050 hole repair at 350 RPM.

Two stages were employed during the hole-filling process: (1) material deposition at the center of the hole without tool-head traverse motion, and (2) sequential traverse movement of the tool head in the +x (length), −x, +y (width), and −y directions over a prescribed distance while material deposition continued. Based on the experimental configuration shown in Fig. 6, a CFD-based process model was developed, as illustrated in Fig. 7, to predict the temperature field, material flow behavior, and strain-rate distribution during the AFSD repair process. These process variables were subsequently used as inputs to the microstructural evolution and material property models to capture the process-dependent characteristics of the repaired region.

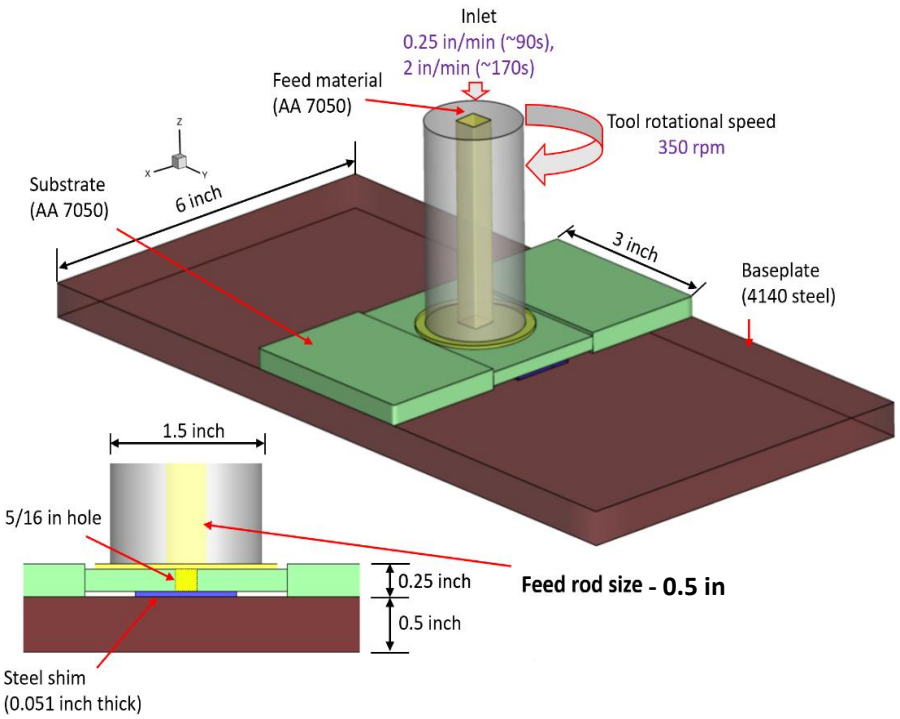


Figure 7 – AFSD CFD model and imposed boundary conditions for simulation of the hole filling process.

The simulation parameters were defined to match the experimental processing conditions. A time-dependent inlet boundary condition was applied at the top surface of the feed material using the prescribed feed-rate history, followed by sequential material deposition along the x- and y-directions according to the tool path and traverse speed specified in the G-code. A stick–slip boundary condition was enforced at the interface between the tool shoulder and the substrate, while full sticking was assumed at the interface between the feed rod and the deposited material. A comparison between the predicted and measured temperature histories for the 350 RPM case is presented in Fig. 8, together with CFD predictions of the temperature evolution during the hole-filling process. The model accurately captures the heating and cooling behavior observed in the thermocouple measurements throughout the repair process. The good agreement between the predicted and measured temperatures demonstrates the high fidelity of the CFD-based AFSD process simulation model and provides confidence in its ability to predict the thermal conditions governing microstructural evolution and material property development during hole repair.

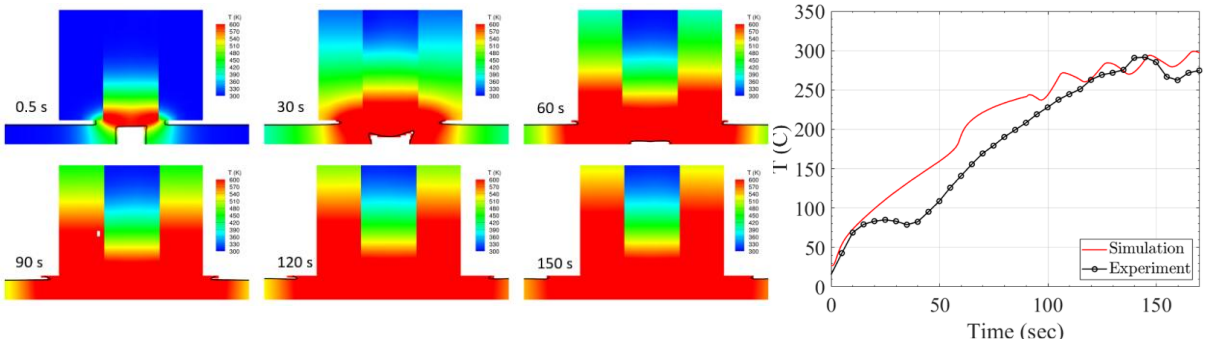


Figure 8 – Evolution of temperature and hole-filling behavior at the mid-plane cross section, and comparison of predicted temperature histories with thermocouple measurements.

3.3 Verification of Microstructure Simulation Model

The temperature and strain-rate fields predicted by the CFD-based AFSD process simulation model were used as inputs to the microstructure simulation module of the PSPP

framework for the 350 RPM case. The predicted shapes of the dynamically recrystallized zone (DXZ), thermo-mechanically affected zone (TMAZ), and heat-affected zone (HAZ) are compared with optical microscopy (OM) observations in Fig. 9. The predicted grain-size distribution and corresponding zone partitioning are shown in Fig. 9(a), while the optical micrograph at the same scale is presented in Fig. 9(b). The boundary of the DXZ is indicated by the green dashed line and was identified based on EBSD analysis, as shown in Fig. 10. The remaining region in Fig. 9(b) is classified as the TMAZ due to the presence of rotated and distorted subgrains resulting from severe plastic deformation during the AFSD process. It can be seen that the predicted shapes and extents of the DXZ and TMAZ are in good qualitative agreement with the OM observations. The comparison demonstrates that the PSPP microstructure model is capable of capturing the spatial distribution of the major microstructural zones formed during the hole-repair process and provides confidence in its ability to predict process-dependent microstructural evolution.

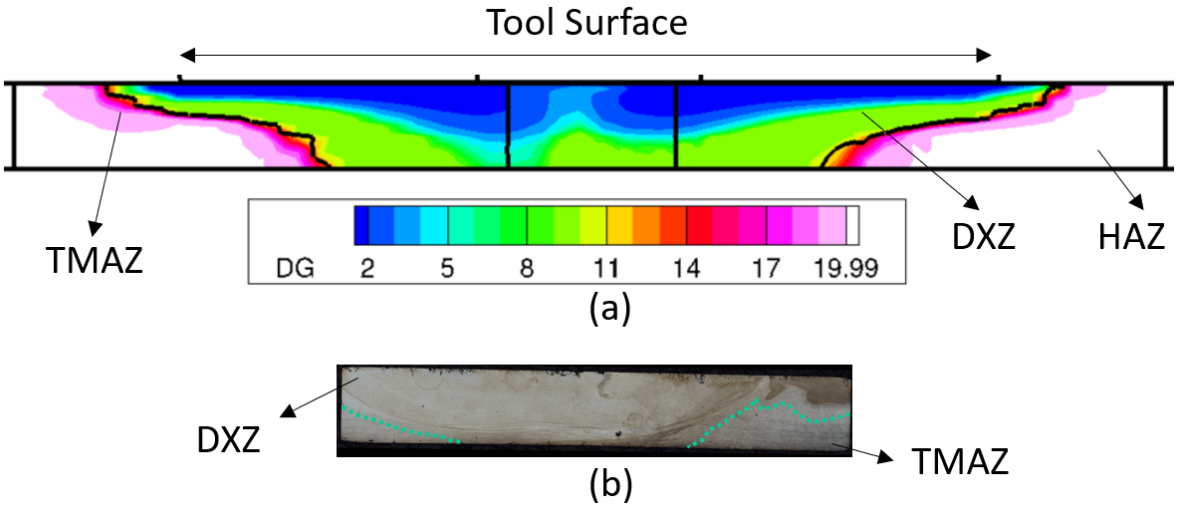


Figure 9 – Comparison of material zones between (a) grain-evolution model predictions and (b) optical microscopy (OM) observations.

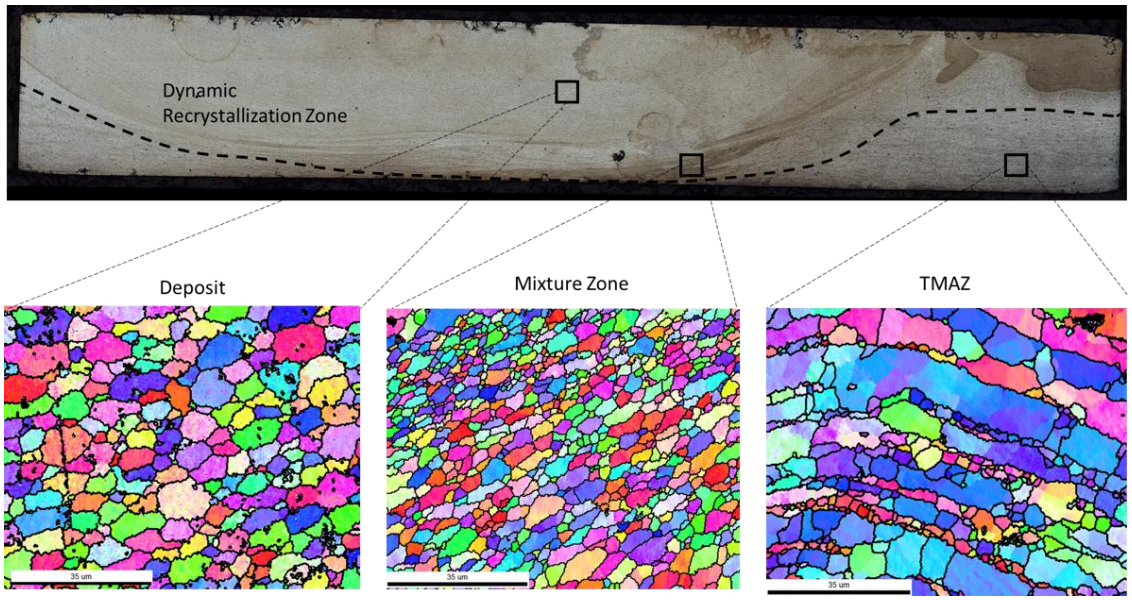


Figure 10 – EBSD characterization of the distinct material zones with the AFSD hole-repair cross section.

Quantitative agreement in the DXZ grain size has not yet been fully achieved. The predicted average grain size in the simulation is 3.59 μm, whereas the grain size measured from OM

and EBSD analyses ranges from approximately 4.7 μm to 6.2 μm. This discrepancy can be attributed, in part, to the fact that the thermo-mechanical fields used to generate the grain-size prediction in Fig. 9(a) do not explicitly account for material feeding and mixing during the deposition process. In addition, the OM and EBSD observations reveal that the microstructural zones within the repaired region are more complex than those represented in the current model. Material within the DXZ may originate from the feed rod, the substrate, or a mixture of both, resulting in local variations in deformation history, thermal exposure, and recrystallization behavior. These material-source-dependent effects can influence grain growth and microstructural evolution and are not fully captured by the present modeling framework. Future improvements to the process simulation will incorporate material-tracking capabilities to better represent feed rod/substrate mixing and further improve the accuracy of grain-size predictions.

As shown in Fig. 10, the deposited zone exhibits a predominantly recrystallized microstructure with a moderate fraction of low-angle grain boundaries (LAGBs). The mixed-material region displays a grain boundary misorientation distribution that closely follows the Mackenzie distribution, indicating a nearly fully recrystallized microstructure. In contrast, the thermo-mechanically affected zone (TMAZ) retains characteristics of the original rolling texture, including elongated grains aligned with the rolling direction. However, evidence of subgrain rotation and the formation of finer banded grains can be observed within this region, indicating that significant plastic deformation and partial microstructural transformation have occurred during the AFSD repair process. These observations suggest that the TMAZ experienced sufficient strain and thermal exposure to promote recovery and localized recrystallization, but not to the extent observed in the deposited and mixed-material regions.

3.4 Precipitate Evolution Prediction for AFSD-Repaired Coupons

Since the primary strengthening mechanism in AA7050 is precipitation hardening, the evolution of precipitates plays a critical role in determining the mechanical performance of the repaired material. The typical precipitation sequence in 7xxx-series aluminum alloys follows:

Supersaturated Solid Solution (SSS) → GP Zones → Metastable η′ → Stable η

The temperature-history-driven evolution of precipitate size, number density, and volume fraction are the key factors governing the strengthening response of the alloy. To capture these effects, a multi-stage precipitation model was implemented within the PSPP framework to predict precipitation evolution during the AFSD hole-repair process. During the initial heating stage, fine η precipitates dissolve as they lose thermodynamic stability at elevated temperatures, resulting in a reduction in the volume fraction of η precipitates. During the subsequent cooling stage, heterogeneous nucleation of η precipitates can occur, and as the temperature decreases below approximately 250°C, GP zones begin to form. During the final natural aging stage, the metastable η′ precipitates nucleate and grow, contributing significantly to the recovery of strength and hardness in the repaired region. Using the thermal history predicted by the CFD-based process model for the 350 RPM case, as shown in Fig. 8, the precipitation model was employed to predict the evolution of precipitate volume fraction and average precipitate radius throughout the repair process. The predicted precipitation evolution is presented in Fig. 11. These results provide the microstructural information required for subsequent material property predictions, including hardness, yield strength, and fatigue performance.

The simulation results indicate that, at the high tool rotational speed of 350 RPM, a portion of the η precipitates dissolves while the remaining precipitates undergo coarsening due to the elevated thermal exposure. The metastable η′ precipitates experience extensive dissolution during the initial high-temperature stage of the repair process. However, following cooling, fine η′ precipitates re-form and grow during the subsequent natural aging stage. Similarly, the GP zones are completely dissolved during material deposition as a result of the elevated temperatures generated by the AFSD process. As the repaired region cools and undergoes natural aging, GP zones re-nucleate and grow, contributing to the recovery of precipitation strengthening. These results demonstrate

the strong influence of the thermal history on precipitation evolution and highlight the importance of accurately predicting temperature fields when assessing the mechanical performance of AFSD-repaired AA7050 components.

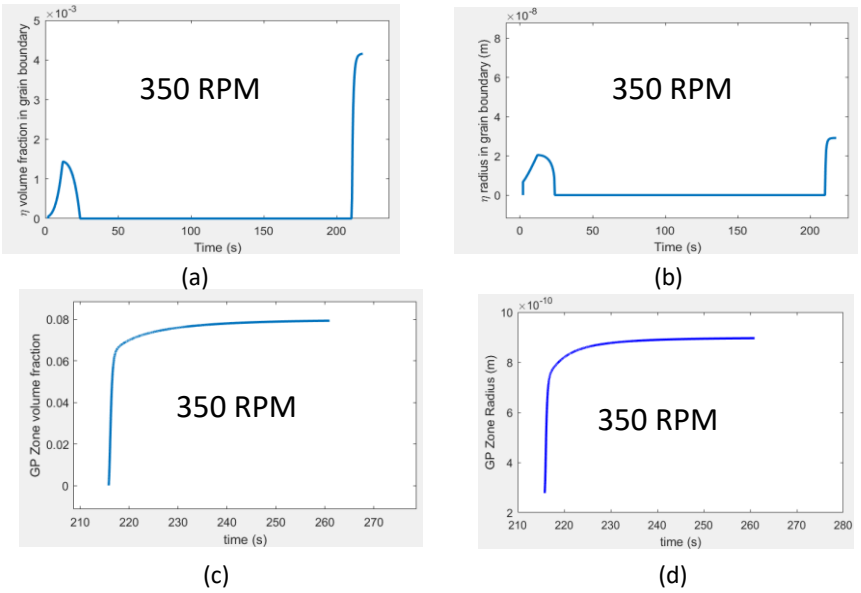


Figure 11 – Predicted evolution of precipitates at a tool rotational speed of 350 RPM: (a) volume fraction and (b) average radius of grain-boundary η precipitates, and (c) volume fraction and (d) average radius of GP zones, as functions of the thermal history during the AFSD hole-repair process.

3.3 Material Property Prediction Using RVE-Based Crystal Plasticity

The microstructural features predicted by the grain-kinetics and precipitation models were incorporated into representative volume elements (RVEs) for crystal plasticity (CP) modeling, as shown in Fig. 12(a). For example, the RVE representing the dynamically recrystallized zone (DXZ) consists of fine equiaxed grains, whereas the RVEs for the thermo-mechanically affected zone (TMAZ), heat-affected zone (HAZ), and base material retain elongated grain morphologies characteristic of the original rolled microstructure.

The constitutive behavior of each material zone was obtained by performing crystal plasticity simulations on the corresponding RVEs, as illustrated in Fig. 12(b). The resulting stress–strain responses capture the effects of local grain morphology and precipitation state on the mechanical behavior of the repaired material. The predicted stress–strain curves for the different material zones were subsequently assigned to the corresponding partitioned regions in the finite element models of the tensile and fatigue test coupons. These zone-specific constitutive properties enable performance predictions that account for the

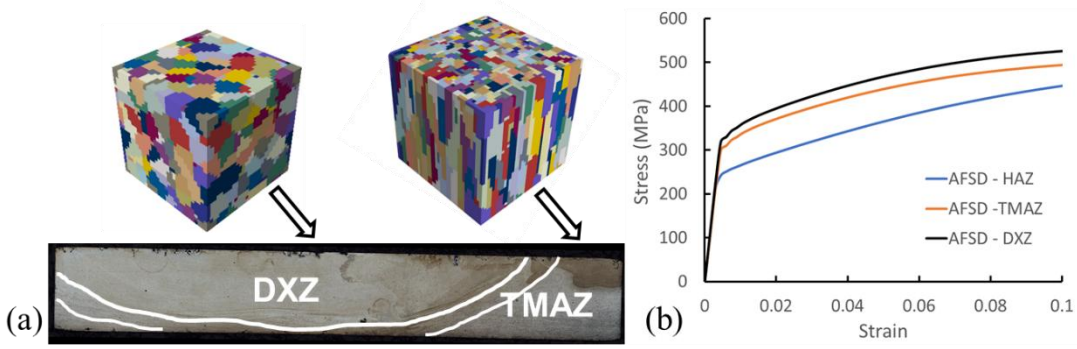


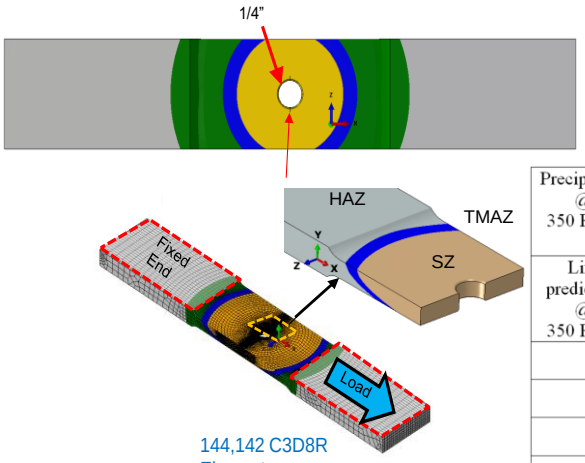
Figure 12 – Representative volume element (RVE) models and corresponding crystal plasticity predictions for the three material zones in the AFSD-repaired coupon: (a) RVE models and (b) predicted stress–strain responses.

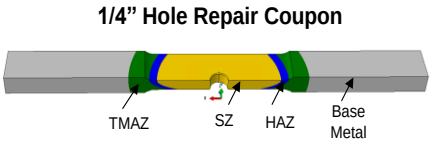
heterogeneous microstructure created during the AFSD repair process and provide the

foundation for crack initiation and fatigue life assessments.

3.4 Performance Evaluation Based on Fatigue Indicator Parameter

We implemented a fatigue indicator parameter (FIP) as the critical link between the AFSD-generated microstructure and fatigue crack initiation life. A transgranular form of the FIP, as defined by Castelluccio and McDowell [23], was employed. The FIP is calculated based on the cyclic plastic shear strain range on a given slip system and the peak normal stress acting on the corresponding slip plane. The maximum FIP value among all grains and slip bands is then used to determine the fatigue crack initiation life. At a high tool rotational speed of 350 RPM, the resulting changes in grain size and precipitate distribution alter the local cyclic plastic deformation behavior. These microstructural changes increase the maximum FIP value, leading to a reduction in crack initiation life. A comparison between the predicted microstructure-driven crack initiation life and the fatigue test results at a stress ratio of R = −1 is presented in Fig. 13 for the 6.35 mm (0.25 in.) AFSD-repaired hole coupons fabricated at a tool rotational speed of 350 RPM.





Precipitates @ 350 RPM	η at grain boundary		GP zones in matrix		η' in matrix	
	Volume fraction	Radius (nm)	Volume fraction	Radius (nm)	Volume fraction	Radius (nm)
	0.00855	37.10	0.0360	1.042	0.0388	2.0

Life prediction @ 350 RPM	Fatigue Indicator Parameter (FIP)	Crack Initiation Life (N_i)
	0.001612	**10,800**

Fatigue Test Data for ¼ in Hole Repaired Coupons at R=-1

Specimen ID	Total Life
HR5.31.22.1	13,546
HR5.31.22.2	9,894
HR5.31.22.6	8,867
HR6.4.22.1	9,267
Average Fatigue Life Test Data	**10,394**

Figure 13 –Summary of the response prediction model and comparison of predicted crack initiation lives with R = −1 fatigue test data for 350 RPM AFSD hole-repaired coupons.

To perform the fatigue analysis, a three-dimensional finite element model was developed in ABAQUS using the material-zone partitioning derived from the CFD-based AFSD process simulation. Zone-specific elastoplastic constitutive properties generated from the crystal plasticity simulations were assigned to the dynamically recrystallized/stir zone (SZ), thermo-mechanically affected zone (TMAZ), and heat-affected zone (HAZ). Following the global structural response analysis, local microstructure-sensitive analyses were performed to determine the FIP distribution and the associated crack initiation life. The maximum predicted FIP value was 0.001612, corresponding to a crack initiation life of 10,800 cycles. Despite the inherent scatter in the fatigue test data, the predicted initiation life is in excellent agreement with the experimentally measured average fatigue life of 10,394 cycles. This result demonstrates the capability of the PSPP framework to establish a quantitative link between AFSD process conditions, microstructural evolution, and fatigue performance, thereby enabling performance-informed process tailoring and optimization.

4. Process Tailoring of AFSD Hole Repair Using the PSPP Framework

After validation of the PSPP tool using a tool rotational speed of 350 RPM, we applied the analysis framework to evaluate two additional tool rotational speeds, 235 RPM and 250 RPM, prior to conducting hole-repair experiments under the analysis-informed process conditions. This study aimed to investigate how variations in tool rotational speed influence the thermal characteristics of the process, with particular emphasis on the peak temperatures achieved and the cooling time, both of which are critical factors governing precipitate evolution and the resulting crack initiation life.

Using the CFD-based process simulation model shown in Figure 7, simulations were performed for the 235 RPM condition. The predicted temperature histories at three thermocouple locations are compared with the experimental measurements in Figure 14. Good agreement between the model predictions and the test data demonstrates the high fidelity and reliability of the PSPP framework in capturing the spatial and temporal variations of the temperature field.

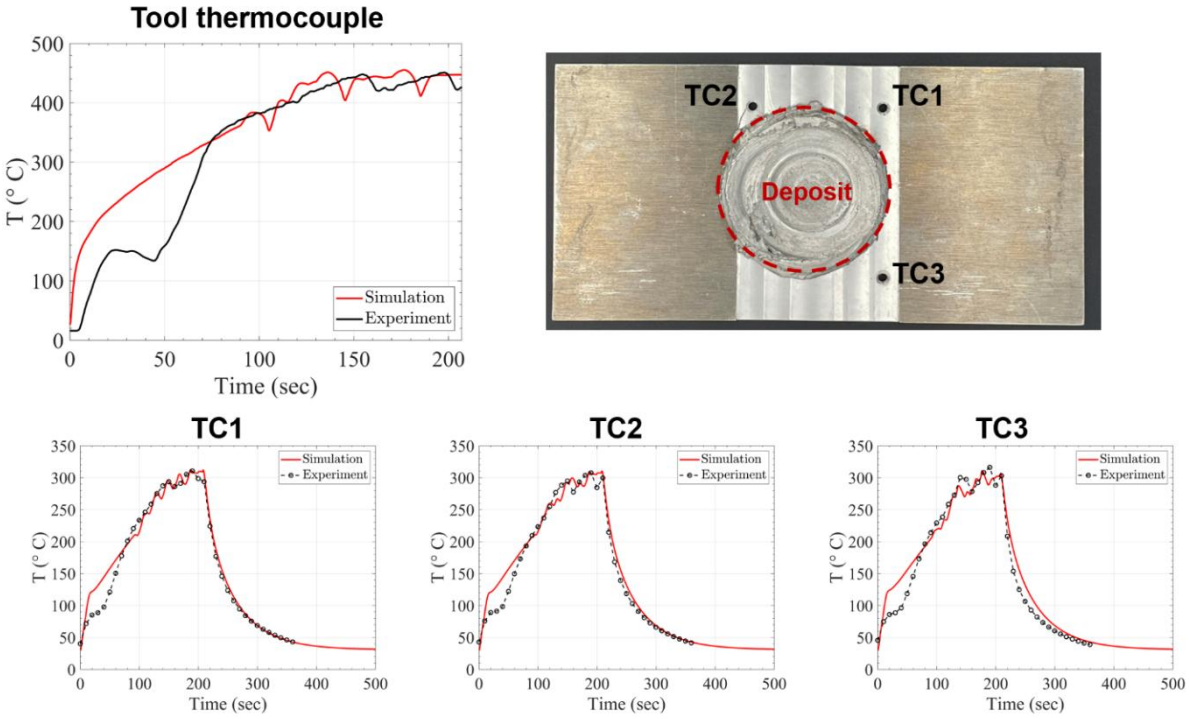


Figure 14 – Comparison of CFD-predicted temperature histories with thermocouple measurements for the constant 235 RPM condition.

At the lower rotational speed of 235 RPM, the material reached a lower peak temperature while still remaining sufficiently high to achieve material plasticization and successful deposition. Compared with the 350 RPM condition, the reduced peak temperatures resulted in a shorter cooling cycle and lower thermal exposure following deposition. These changes in the thermal history significantly affect the precipitation kinetics and microstructural evolution of the repaired material. By understanding how tool rotational speed influences the thermal response, the PSPP framework can be used to predict and tailor precipitate evolution, thereby optimizing the resulting microstructure and improving crack initiation life.

Table 1 - Summary of the precipitate types, volume fractions, and radii for three RPMs

Precipitates / RPM	η at grain boundary		GP zones in matrix		η' in matrix	
	Volume fraction	Radius (nm)	Volume fraction	Radius (nm)	Volume fraction	Radius (nm)
235 RPM in L3	0.00347	27.46	0.0363	0.893	0.043	2 nm
250 RPM in L3	0.00365	27.93	0.0363	0.894	0.043	2 nm
350 RPM in L3	0.00416	29.17	0.0361	0.929	0.0392	2 nm

To further validate the rationale for selecting a tool rotational speed of 235 RPM, an additional process simulation and corresponding AFSD hole-repair experiment were conducted at 250 RPM. The CFD-predicted thermal histories for the three rotational speeds (235, 250, and 350 RPM) were subsequently used as inputs to the precipitation model. The resulting precipitate characteristics, including precipitate type, volume fraction, and average radius, are compared in Table 1. This

comparison provides insight into the influence of tool rotational speed on precipitate evolution and the associated microstructural state of the repaired material.

At the higher rotational speed of 350 RPM, the microstructure exhibits a greater volume fraction and larger size of overgrown precipitates along the grain boundaries. In contrast, the volume fractions and sizes of the strengthening GP zones and η′ precipitates are reduced. Since GP zones and η′ precipitates provide significant resistance to dislocation motion and contribute substantially to precipitation hardening, their reduction leads to a deterioration in mechanical performance. The formation of coarse grain-boundary precipitates consumes a significant amount of Mg and Zn solute atoms, leaving fewer solute atoms available for the nucleation and growth of the fine GP zones and η′ precipitates within the grains. Consequently, the 350 RPM condition is expected to exhibit inferior material performance compared with the 250 RPM and 235 RPM conditions from a precipitation-hardening perspective.

To further support this physical interpretation, two key microstructure-sensitive response parameters predicted by the crystal plasticity-based constitutive model were examined: the resolved resistance stress to dislocation motion, χ_a, and the fatigue indicator parameter (FIP). The predicted distributions of these parameters for the different rotational speeds are presented in Figure 15. A higher value of χ_a indicates greater resistance to plastic deformation due to stronger precipitate strengthening, whereas a lower FIP corresponds to reduced local cyclic plasticity and improved resistance to fatigue crack initiation. Together, these metrics provide quantitative evidence linking precipitate evolution to the fatigue performance of the AFSD-repaired material.

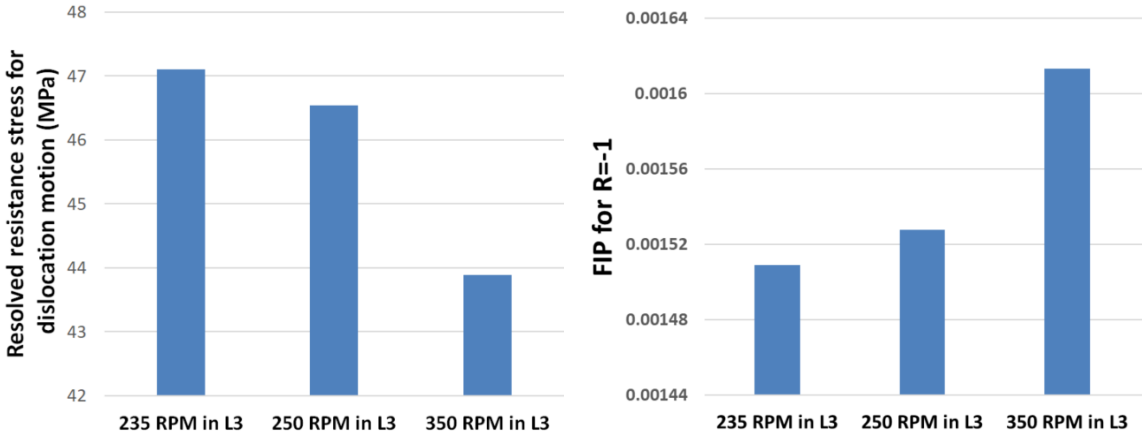


Figure 15 – Effects of tool rotational speed on microstructural properties: (a) resolved resistance stress to dislocation motion, χ_a, and (b) fatigue indicator parameter (FIP).

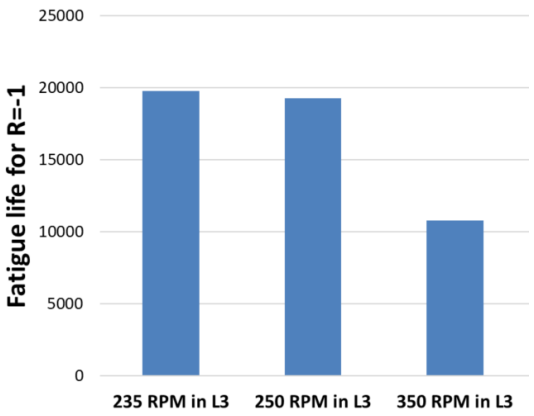


Figure 16 –Comparison of predicted crack initiation lives at three different tool rotational speeds.

Superior fatigue performance is expected at 235 RPM, as evidenced by the highest resolved resistance stress for dislocation motion, χa, of 47.1 MPa and the lowest fatigue indicator parameter (FIP) value of 0.0015. Based on the framework developed by Castelluccio and McDowell [23], the

FIP serves as a local measure of cyclic fatigue damage accumulated within a grain. The fatigue crack initiation life is inversely related to the magnitude of the maximum FIP, as illustrated in Figure 15. The predicted crack initiation lives corresponding to the three rotational speeds are presented in Figure 16. The fatigue crack initiation life decreases from approximately 19,800 cycles at 235 RPM to 10,800 cycles at 350 RPM, representing a reduction of nearly 45%. This trend is consistent with the precipitation-informed crystal plasticity predictions. As the rotational speed increases, the higher thermal exposure promotes the dissolution and coarsening of strengthening η′ precipitates, reducing the resolved resistance stress for dislocation motion from approximately 47.1 MPa to 43.9 MPa. The lower slip resistance leads to increased cyclic plastic strain accumulation and a corresponding increase in the maximum FIP from 1.51×10^{-3} to 1.61×10^{-3}.

5. Summary and Conclusions

This study presents a multiphysics modeling framework to establish the process–structure–property–performance (PSPP) relationship for AFSD-based solid-state repair of corroded fastener holes in AA7050 coupons. The PSPP framework consists of a chain of sequentially coupled models that predict the thermal-fluid dynamics of the AFSD process, microstructural evolution, the resulting heterogeneous mechanical properties, and the corresponding fatigue performance. The physics-based framework demonstrates the capability to capture the complex thermal, metallurgical, and mechanical phenomena governing AFSD repair.

Each solution module within the PSPP framework was validated using experimental data obtained from AFSD-repaired AA7050 hole coupons fabricated at a tool rotational speed of 350 RPM. The validated framework was subsequently applied to identify process conditions that maximize fatigue crack initiation life. The results showed that improved fatigue performance can be achieved by tailoring the process window to provide sufficient heat input and plastic deformation for complete bonding and defect-free deposition while minimizing excessive thermal exposure that promotes η′ precipitate dissolution and grain-boundary η coarsening. The optimized thermal–mechanical condition increases resistance to cyclic plastic deformation, reduces the fatigue indicator parameter (FIP), and consequently extends fatigue crack initiation life.

The developed PSPP framework can be readily extended from AFSD repair to AFSD-based additive manufacturing through layerwise deposition. By integrating CFD-based process simulation, microstructure evolution models, crystal plasticity, and fatigue performance prediction, the framework enables quantitative assessment of the effects of deposition parameters, thermal cycling, and layer interactions on the resulting microstructure, mechanical properties, and structural performance. Such a capability provides a foundation for physics-informed process optimization and digital engineering-enabled qualification of AFSD-manufactured components.

Future efforts will focus on extending the PSPP framework to the fabrication of large-scale aluminum structures through AFSD. Physics-based machine learning surrogates and inverse-design methodologies are currently being developed to accelerate PSPP predictions and enable rapid identification of optimal fabrication plans and deposition strategies that satisfy specified performance requirements. These capabilities will support performance-informed manufacturing and digital engineering-enabled qualification of next-generation AFSD-fabricated aerospace structures.

6. Acknowledgement

This work is funded by Naval Air Warfare Center. Aircraft Division under the Contract of N68335-23-C-0115. The views and conclusions contained in this document are those of the authors and should not be interpreted as representing the official policies, either expressed or implied, of NAVAIR or the U.S. Government.

7. Contact Author Email Address

jlua@gem-innovation.com

8. Copyright Statement

The authors confirm that they, and/or their company or organization, hold copyright on all of the original material

included in this paper. The authors also confirm that they have obtained permission, from the copyright holder of any third party material included in this paper, to publish it as part of their paper. The authors confirm that they give permission, or have obtained permission from the copyright holder of this paper, for the publication and distribution of this paper as part of the ICAS proceedings or as individual off-prints from the proceedings.

References

[1] Naval Aviation Enterprise, “Naval Aviation Enterprise Corrosion Prevention Team”, Washington, DC, USA, 2009.

[2] Gottwald, R. B., Griffiths, R. J., Petersen, D. T., Perry, M. E. J., and Yu, H. Z., “Solid-state metal additive manufacturing for structural repair,” Acc. Mater. Res., Vol. 2, no. 9, pp. 780–792, Sep. 2021.

[3] Rahito, D., Wahab, A., and Azman, A. H., “Additive manufacturing for repair and restoration in remanufacturing: an overview from object design and systems perspectives,” Processes, Vol. 7, no. 11, Art., no. 11, Nov. 2019.

[4] Chen, Z., Duan, Y., Wang, P., and Qian, H., “Residual stress redistribution analysis in the repair welding of AA6082-T6 aluminum alloy joints: Experiment and Simulation,” Materials, vol. 15, no. 18, Art. no. 18, 2022.

[5] Li, S., et al., “Effect of repair welding on microstructure and mechanical properties of 7N01 aluminum alloy MIG welded joint,” Journal of Manufacturing Processes, vol. 54, pp. 80–88, Jun. 2020.

[6] Griffiths, R. J., Garcia, D., Hahn, G. D., Lua, J., Phan, N., and Yu, H. Z., “A non-melting additive approach to structural repair of aluminum aircraft fastener holes.” Additive Manufacturing, Oct. 2024.

[7] Yu, H. Z. et al., “Non-beam-based metal additive manufacturing enabled by additive friction stir deposition,” Scripta Materialia, Vol. 153, pp. 122–130, Aug. 2018.

[8] Palya, N. I., Fraser, K. A., Hong, Y., Zhu, N., Williams, M. B., Doherty, K., Allison, P. G., and Jordon, J. B., “Multi-physics approach to predict fatigue behavior of high strength aluminum alloy repaired via additive friction stir deposition,” Integr. Mater. Manuf. Innov. Vol. 12. Pp. 441-455, 2023.

[9] Yu, H. Z., *Additive friction stir deposition*, Elsevier, 2022.

[10] Yoder, J. K., Griffiths, R. J., and Yu, H. Z., “Deformation-based additive manufacturing of 7075 aluminum with wrought-like mechanical properties,” Materials & Design, Vol. 198, p. 109288, Jan. 2021.

[11] Martin, L. P., Luccitti, A., and Walluk, M., “Repair of aluminum 6061 plate by additive friction stir deposition,” Int J Adv Manuf Technol, Vol. 118, no. 3, pp. 759–773, Jan. 2022.

[12] Griffiths, R. J., Petersen, D. T., Garcia, D., and Yu, H. Z., “Additive friction stir-enabled solid-state additive manufacturing for the repair of 7075 aluminum alloy,” Applied Sciences, Vol. 9, no. 17, Art. no. 17, Jan. 2019.

[13] Feng, B., Rajanna, M. R., Lua, J., Hahn, G., Knight, K., Murray, G., Timmons, A., and Phan, N., “Multi-stage precipitation modeling for AA 7050 hole repairs in additive friction stir deposition, J. Appl. Phys. 136, 2024, 165102.

[14] Wang, Z., Wang, B., Li, Z., Guo, S., Shen, Z., Xu, M., Chen, Y., Xie, G., Guo, Y., Liu, X., Hou, W., Piao, Z., Yan, S., Shah, L., Liang, D., and H. Li, H., “Microstructure evolution and fatigue properties of additive friction stir deposited Al-Mg-Si alloy,” J. Alloy. Compd. 1044, 2025.

[15] Zhu, N., T. Hickok, K.A. Fraser, D., Yu, Y., Chen, K., An, L.N., Brewer, P.G., Allison, and J. B., Jordon, J. B., “Neutron diffraction analysis of residual stress distribution in the lubricant-free TR-AFSD AA7075 repair coupled with SPH simulations,” J. Adv. Joining Processes 11, 2025, 100283.

[16] Jabbar, H., Taylor, A., Biniyazan, F., Grubbs, J., B. Sousa, B., and S. Beck, S., “A process-structure-property ICME framework for additive friction stir deposition repair of aluminum alloys,” Materials & Design 266, 2026, 116168.

[17] Li, X., Rajanna, M. R., Lua, J., Timmons, A., Murray, G., Phan, N., and R. Eberheim, R., “Computational fluid dynamics simulation for additive friction stir deposition of aluminum alloy,” 79th Annual Forum & Technology Display, West Palm Beach, FL, May 16-18, 2023.

[18] Myhr, O. R., and Grong, O., “Modelling of non-Isothermal transformations in alloys containing a particle distribution.” Acta Materialia, Vol. 48, No. 7, pp. 1605–1615, 2000.

[19] Hill, R. “Generalized Constitutive Relations for Incremental Deformation of Metal Crystals by Multislip.” Journal of the Mechanics and Physics of Solids, Vol. 14, No. 2, pp. 95–102, 1966.

[20] Xue, Y., McDowell, D. L., Horstemeyer, M. F., Dale, M. H., and Jordon, J. B. “Microstructure-based multistage fatigue modeling of aluminum alloy 7075-T651.” Engineering Fracture Mechanics, Vol. 74, No. 17, 2007, pp. 2810–2823, 2007.

[21] Shi, J., Chopp, D., Lua, J., Sukumar, N., and Belytschko, T. “Abaqus implementation of extended finite element method using a level set representation for three-dimensional fatigue crack growth and life predictions.” Engineering Fracture Mechanics, Vol. 77, No. 14, pp. 2840–2863, 2010.

[22] Sadeghirad, A., Chopp, D. L., Ren, X., Fang, E., and Lua, J. “A novel hybrid approach for level set characterization and tracking of non-planar 3D cracks in the extended finite element method,” Engineering Fracture Mechanics, Vol. 160, pp. 1–14, 2016.

[23] Castelluccio, G. M., and McDowell, D. L., “Assessment of small fatigue crack growth driving forces in single crystals with and without slip bands,” International Journal of Fracture, Vol. 176, No. 1, pp. 49–64, 2012.